Supporting Information: Hydrogen Evolution from Pt/Ru-Coated p-Type WSe_2 Photocathodes

James R. McKone, Adam P. Pieterick, Harry B. Gray*, and Nathan S. Lewis*

*Corresponding authors: hbgray@caltech.edu; nslewis@caltech.edu

Division of Chemistry and Chemical Engineering and the Joint Center for Artificial Photosynthesis, California Institute of Technology, 1200 East California Blvd, Pasadena, CA 91125

S.1. Mott-Schottky methodology and data

Mott-Schottky data were collected using a standard procedure that involved measurement of the differential capacitance over a range of voltages for which the WSe_2 electrode was in reverse bias. DC potentials were scanned from -0.800 to 0.200 V versus SCE, in the presence of a superimposed 10 mV RMS amplitude AC signal having a frequency of 20, 50, or 100 kHz, respectively. The differential capacitance was calculated for each frequency using the relationship:

$$Z'' = \frac{1}{2\pi f C_{\text{diff}}} \qquad \text{(Eq. S1)}$$

where Z'' is the imaginary value of the impedance (calculated automatically by the Gamry Echem Analyst software package), C_{diff} is the differential capacitance, and f is the frequency of the applied signal. This relationship holds for AC frequencies sufficiently high that the current-voltage characteristics are dominated by the semiconductor space-charge region (thus faradaic processes and the Helmholtz capacitance can be ignored). For frequencies ≥50 kHz, p-WSe_2 photoelectrodes that were evaluated using this approach generally yielded linear relationships between the applied DC potential and C_{diff}^{-2} over the potential range from -0.5 to 0.25 V vs. SCE, indicating that the aforementioned condition existed in this potential range.

Figures S1 and S2 illustrate the full results of Mott-Schottky measurements on 9 different p-WSe_2 electrodes in contact with the ferricyanide-ferrocyanide redox couple at three different pH values from 2.5-10.2. The electrodes tended to cluster into two different distributions, one in which the flat-band potentials varied by <0.1 V over the full range of pH 2.5-10.2, and another in

which the flat-band potentials varied by >0.1 V over the same range of pH values. All of the electrodes showed a relatively small changes in their flat-band potential from pH 2.5-6.6, and only those with prominent visible step edges showed a significant negative shift in their flat-band potentials in the pH 6.6-10.2 range.

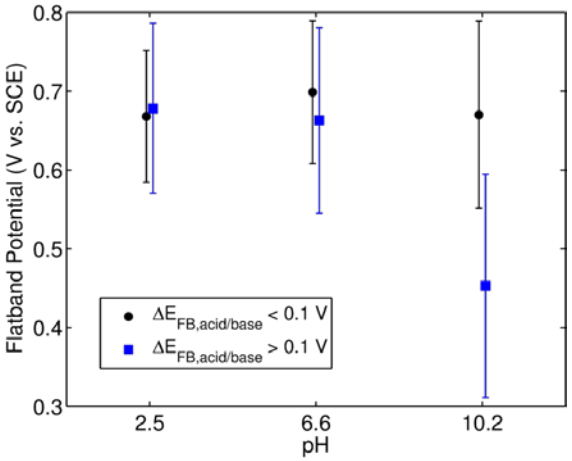

Figure S1. Averaged Mott-Schottky results for 9 different p-WSe_2 photoelectrodes in contact with aqueous $Fe(CN)_6^{3-/4-}$ redox couple. Blue squares are for five electrodes exhibiting a variation in flat-band potential, $\Delta E_{FB,acid/base}$ > 0.1 V from pH 2.5 to pH 10.2; whereas black circles are for four electrodes exhibiting $\Delta E_{FB,acid/base}$ < 0.1 V over the same pH range. Error bars are shown at the 1σ confidence interval.

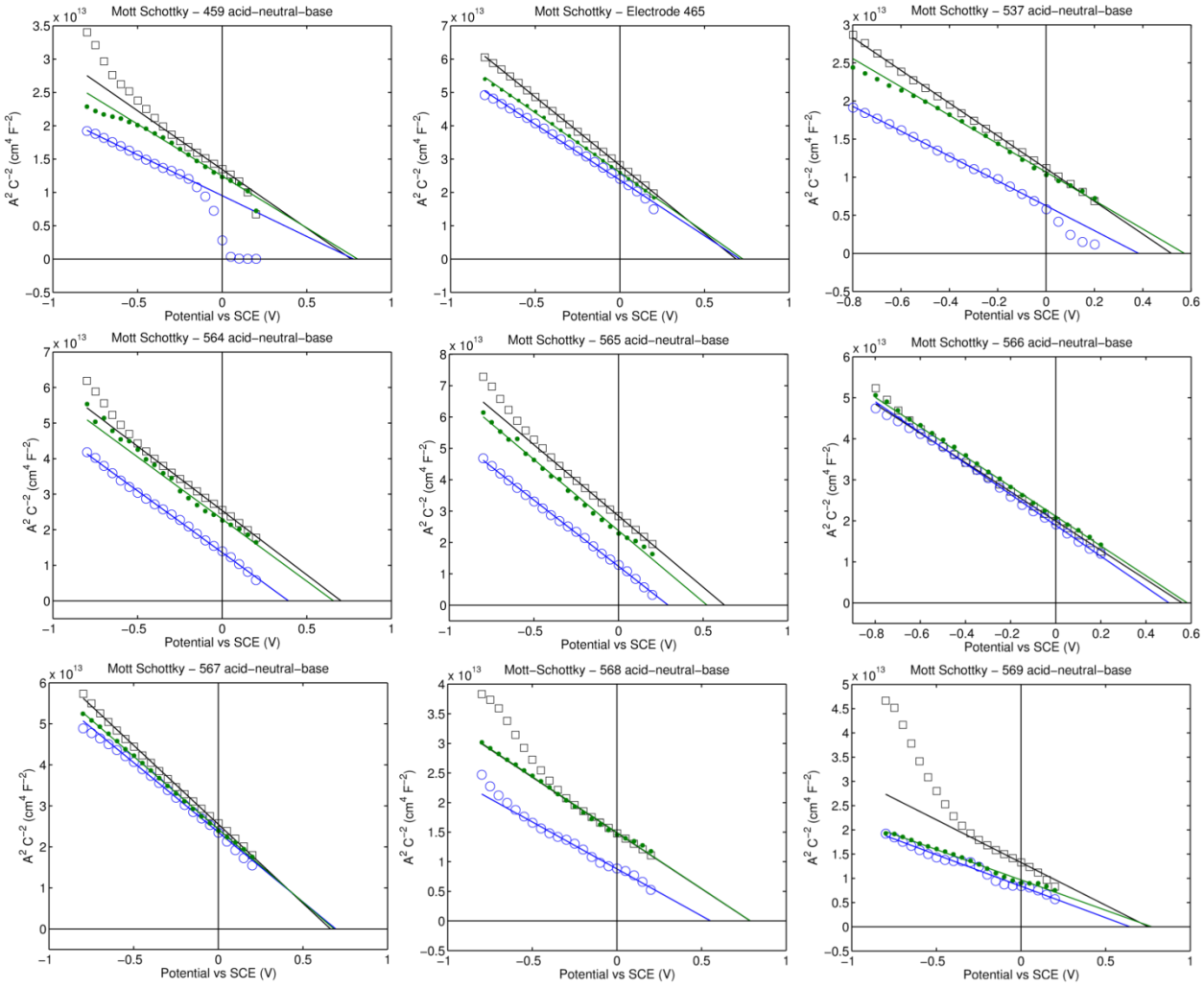

Figure S2. Collected Mott-Schottky data for 9 different p-WSe_2 electrodes in contact with aqueous $Fe(CN)_6^{3-/4-}$ redox couple at three different pH values. For all data shown, pH values are as follows: black squares 2.5; green filled circles 6.6; blue open circles 10.2. Note that electrode 459 (upper left) was tested after having been deposited with Ru/Pt catalyst, which might explain the large deviation from linearity at relatively positive potentials compared with the other electrodes.

S.2. Catalyst Deposition

Figure S3 displays the current vs time traces for representative photoelectrochemical depositions of Pt and Ru, respectively, on the p-WSe_2 surface. In both cases, potentiostatic deposition resulted in a low-current induction period (which was more pronounced for Ru) followed by a rapid increase in cathodic current density that corresponded to vigorous hydrogen evolution concurrent with metal deposition.. This H_2 evolution was evidenced by the appearance of bubbles on the electrode surface along with the observed increase in current density.

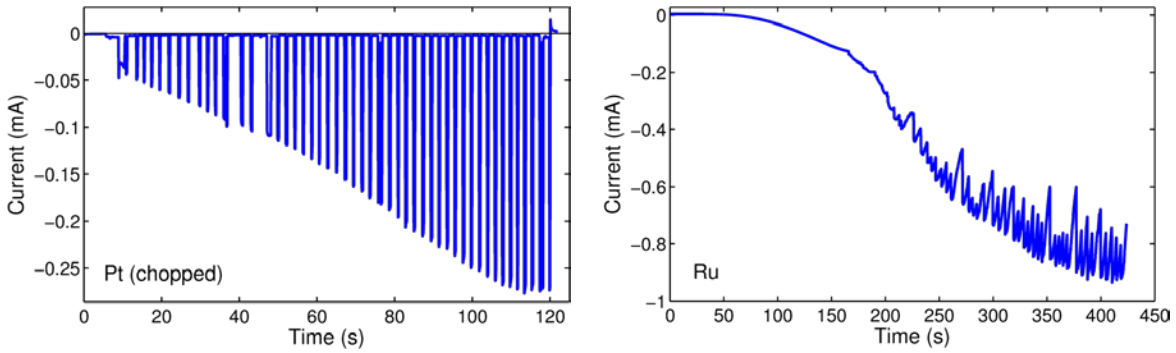

Figure S3. – Current vs time plots for depositions of Pt (left) and Ru (right) on illuminated p-WSe_2 under potentiostatic bias of -0.1 V vs. SCE. The Pt deposition proceeded with manually chopped illumination, whereas the Ru deposition had continuous illumination.

Figure S4 shows a scanning electron micrograph of a p-WSe_2 photoelectrode that had been decorated with a Pt electrocatalyst. The metal deposited as nanoparticles over the entire electrode surface, with preferential deposition of continuous "nanowires" along the step edges of the crystal. This behavior is quite similar to that previously observed for metal deposition on highly-ordered pyrolytic graphite.[1] We were unable to determine whether the Ru/Pt co-deposition, as described in the main text, resulted in mixed-metal nanoparticles or in discrete particles of each metal type, due to the small size of the particles compared to the sampling area of, e.g., energy dispersive spectroscopy integrated in an electron microscope. Nevertheless, the mechanism of electrodeposition (and possibly electroless deposition for Pt) is of interest for future studies.

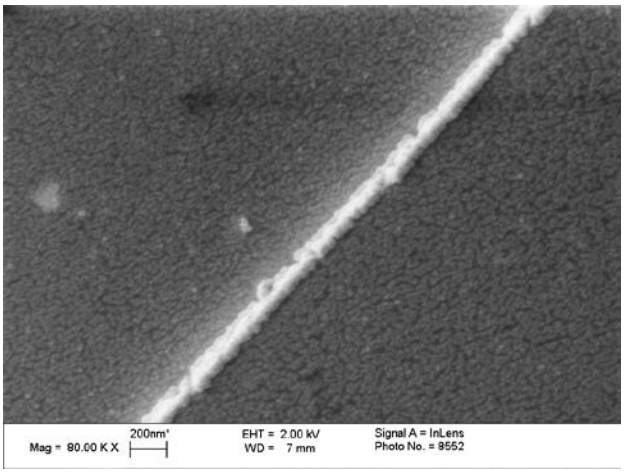

Figure S4. Scanning electron micrograph of p-WSe_2 coated with Pt electrocatalyst.

S.3. Effective diffusion length calculation

Calculations of the effective minority-carrier diffusion length (L_D) for p-WSe_2 made use of the well-established Gärtner model for carrier diffusion in crystalline semiconductors. This model has been used previously to analyze the behavior of WSe_2 photoelectrodes.[2] In the present study, the internal quantum yield was determined according to equation S2

$$\Phi_{\text{int}} = 1 - \frac{e^{-\alpha W}}{1+\alpha L_D} \qquad \text{(Eq. S2)}$$

where Φ_{int} is the internal quantum yield, α is the (wavelength-dependent) absorption coefficient, and W is the depletion width of the semiconductor. The value of W for the p-WSe_2 electrodes was estimated as 50 nm, based on the doping level implied by the Mott-Schottky data.

Reliable absorption coefficient data for p-WSe_2 are not available over the full range of visible to near-IR wavelengths. We therefore used the normalized external quantum yield ($\Phi_{ext}/\Phi_{ext,max}$) in place of Φ_{int}, and light absorption data taken from a previous publication.[2] Normalization of the Φ_{ext} data to its maximum value has the effect of approximating the Φ_{int} under the assumption that the Φ_{ext} maximum is limited only by solution absorption and optical reflection. As shown in the main text (Figure 9), the Gärtner-modeled normalized Φ_{ext} values corresponding to a L_D value of 1 μm fit well to the experimental data, whereas L_D = 0.5 or 2 μm do not fit well, implying a reasonable confidence interval within the limitations of the simple approximation used in the data analysis.

S.4. Comparison of light sources

Figure S5 depicts the respective photon spectral distribution for the ELH-type tungsten halogen lamp (hereafter referred to simply as ELH) used in the present study, as well as the spectral distribution of the AM 1.5G reference spectrum. The shaded portions of the plots are the convolution of the spectral response data shown in the main text (Figure 8) with the spectra of the respective light sources. Qualitatively, the ELH and AM 1.5G spectra are similar, exhibiting broad intensity over the visible wavelengths from 400-800 nm. However, the ELH spectrum contains a larger proportion of intensity in the 500-800 nm wavelength range, and less intensity in the near-IR region, compared to the AM 1.5G spectrum. Thus, characterization of photoelectrodes that have a spectral response dominated by the visible wavelengths (such as WSe_2) using an ELH lamp tends to overestimate the current density relative to what would be observed using AM 1.5G illumination, as illustrated in Figure S5. The difference, however, is small enough that semiconductors identified as promising using ELH radiation are also promising for "real-world" solar applications. Notably, in the limit of very high quantum efficiencies (approaching unity) above the p-WSe_2 bandgap, the predicted photocurrent densities for AM 1.5G and ELH radiation sources both approach values of >40 mA cm^{-2}.

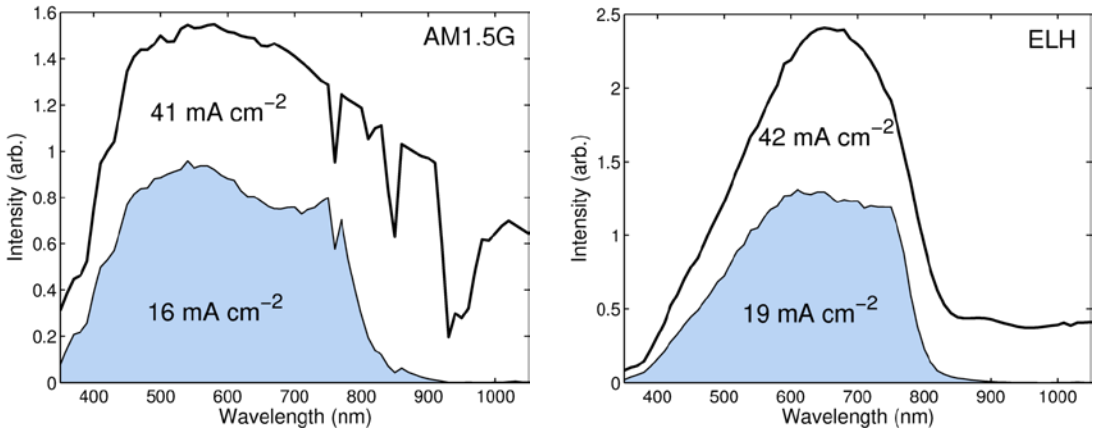

Figure S5. Spectral response behavior for p-WSe_2 photoelectrodes convoluted with the spectra of AM1.5G (left) and ELH (right) radiation sources in the wavelength range 350-1050 nm. The upper solid lines correspond to the full spectra, whereas the shaded areas correspond to the portion of those spectra expected to contribute to productive photocurrent for p-WSe_2 in contact with 50 mM methyl viologen solution based on spectral response measurements. The associated current density values are the predicted photocurrent densities from spectral response (inside shaded area) and unity quantum yield across the spectral region (combined shaded and un-shaded areas), respectively.

S.5. Energy-conversion efficiency measurements

Photoelectrochemistry experiments carried out in the manner described in the main text using a three-electrode cell are useful for the independent assessment of the energy saved by a photocathode relative to the Nernst potential of the solution (i.e. independent of the composition, reactivity, and kinetics of the counter electrode). Under the specific conditions where the solution maintains a constant pH value and is saturated with H_2(g) at 1 atm pressure, the Nernst potential of the solution is the thermodynamic potential for hydrogen evolution (RHE), and the *J-E* characteristics of the photocathode under such condition can be expressed in terms of energy-conversion efficiency relative to the thermodynamic potential for hydrogen evolution.

Full water splitting using a WSe_2 photocathode, or another semiconductor with a band gap lower than ~1.8 eV, requires additional bias that could be provided either by an external voltage source (e.g. a potentiostat), or by a second photoelectrode connected in series with the photocathode. Independent 3-electrode experiments on photocathodes and anodes (either photoanodes or "dark" anodes) tested under the same conditions can be overlaid on the same voltage axis to yield predictions of the operating voltage and/or current density of a full water splitting device.[3] The three-electrode methodology yields considerably more information about components of a water splitting cell than a two-electrode experiment, as it does not convolute the thermodynamic and kinetics factors of two half-reactions into one measurement. Thus, we have used three-electrode experiments for the reported studies of p-WSe_2 energy conversion properties under hydrogen-evolution condition and in contact with reversible redox couples. Two-electrode experiments, e.g. as described by Chen et al.,[4] are also useful, but only when trying to evaluate the performance of full water-splitting device. In such a case the characteristics of both the cathode and anode directly affect the measured performance of the system of interest. To clearly differentiate between full cell and half-cell measurements, the former are denoted as cell efficiencies, while the latter are denoted as photoelectrode efficiencies, which are the values reported herein.

S.6. Collected energy-conversion figures of merit

Table S1 below contains collected energy-conversion figures of merit for p-WSe_2 photoelectrodes under hydrogen-evolution conditions as well as in contact with $Ru(NH_3)_6^{3+/2+}$ solution.

TABLE S1

Electrode #	Catalyst	Electrolyte*	V_{oc} (mV)	J_{sc} (mA cm-2)	Fill Factor	Efficiency (%)
412A	Ru	KHP	660	-16.3	0.31	3.3
459A	Ru	KHP	585	-18.2	0.17	1.8
400	Pt	KHP	610	-19.2	0.53	6.2
414	Pt	KHP	590	-15.4	0.30	2.8
415	Pt	KHP	570	-20.3	0.44	5.1
459C	Ru/Pt	H_2SO_4	500	-14.1	0.55	3.9
463	Ru/Pt	H_2SO_4	525	-20.5	0.53	5.6
464	Ru/Pt	H_2SO_4	610	-22.1	0.52	7.0
412B	Ru/Pt	KHP	620	-16.8	0.49	4.5
458A	Ru/Pt	KHP	635	-21.7	0.45	6.1
458B	Ru/Pt	KHP	630	-22.6	0.48	6.8
459B	Ru/Pt	KHP	630	-24.5	0.46	7.2
465	None	RuHex	515	-14.7	0.43	3.3
537	None	RuHex	505	-17.1	0.42	3.6
566	None	RuHex	420	-16.8	0.23	2.0

*KHP refers to 0.5 M K_2SO_4 buffered with 0.2 M potassium hydrogen phthalate at pH ~4.2; H_2SO_4 refers to 0.5 M sulfuric acid; RuHex refers to 50 mM $Ru(NH_3)_6^{3+/2+}$ solution buffered to pH 2.25 using 0.5 M potassium phosphate.

Supporting References

(1) Favier, F.; Walter, E. C.; Zach, M. P.; Benter, T.; Penner, R. M. *Science* **2001**, *293*, 2227.

(2) Jakubowicz, A.; Mahalu, D.; Wolf, M.; Wold, A.; Tenne, R. *Phys. Rev. B* **1989**, *40*, 2992.

(3) Walter, M.; Warren, E.; McKone, J.; Boettcher, S.; Qixi, M.; Santori, L.; Lewis, N. *Chem. Rev.* **2010**, *110*, 6446.

(4) Chen, Z.; Jaramillo, T. F.; Deutsch, T. G.; Kleiman-Shwarsctein, A.; Forman, A. J.; Gaillard, N.; Garland, R.; Takanabe, K.; Heske, C.; Sunkara, M.; McFarland, E. W.; Domen, K.; Miller, E. L.; Turner, J. a.; Dinh, H. N. *J. Mater. Res.* **2011**, *25*, 3.